Chemical Engineering Journal 160 (2010) 398–407

Contents lists available at ScienceDirect

Chemical Engineering Journal

journal homepage: www.elsevier.com/locate/cej

Adsorption equilibria and kinetics of CO_2 and N_2 on activated carbon beads

Chunzhi Shen[a,b], Carlos A. Grande[b], Ping Li[a], Jianguo Yu[a], Alirio E. Rodrigues[b,*]

[a] State Key Laboratory of Chemical Engineering, College of Chemical Engineering, East China University of Science and Technology, Shanghai 200237, China
[b] Laboratory of Separation and Reaction Engineering (LSRE), Associate Laboratory LSRE/LCM, Department of Chemical Engineering, Faculty of Engineering, University of Porto, Rua Dr. Roberto Frias, s/n, 4200-465, Porto, Portugal

ARTICLE INFO

Article history:
Received 1 July 2009
Received in revised form 4 November 2009
Accepted 3 December 2009

Keywords:
Adsorption
Carbon dioxide
Pitch-based activated carbon
Virial model
Multisite Langmuir
Breakthrough curve

ABSTRACT

Knowledge of adsorption equilibria and kinetics of pure gases is required for designing an adsorption process for a new material that can be scaled-up to large amounts. In this work, adsorption equilibrium data of CO_2 and N_2 on pitch-based activated carbon (AC) beads at 303, 333, 363, 393, and 423 K ranging from 0 to 100 kPa and at 303, 333 K ranging from 0 to 4000 kPa were presented. The adsorption capacity is 1.918 mol/kg for CO_2 and 0.270 mol/kg for N_2 at 303 K and 100 kPa. The full set of data was fitted with both Virial adsorption equation and multisite Langmuir model. The diffusion of single gases in the microporous structure of AC beads was studied by diluted breakthrough experiments performed over the same temperature range of 303–423 K. A mathematical model was employed in the simulation of breakthrough curves. It was determined that for CO_2 and N_2, the controlling mechanism is micropore diffusion. The micropore diffusivity constant (D_c/r_c^2) for carbon dioxide and nitrogen obtained at 303 K is 1.058×10^{-2} and 7.185×10^{-2} s^{-1}, respectively. The data reported in this work allows modeling of any adsorption processes with this new material.

1. Introduction

Carbon dioxide from flue gas emitted by power plants, steel mills, and cement kilns is responsible for a considerable amount (90%) of the total anthropogenic CO_2 emissions throughout the world, which causes global climate change [1]. One of the alternatives to mitigate carbon dioxide emissions from fossil fuel plants is to capture CO_2 from its original source and store it safely in secure geological formations. The two general approaches to reduce carbon emissions from existing plants are post-combustion capture and oxy-combustion, while pre-combustion is used at new power plants that employ integrated gasification combined cycle (IGCC) technology. Commercial CO_2 capture technologies that exist today, such as sequestration by direct injection into geologic, or monoethanolamine (MEA) chemical absorption, are energy intensive and expensive. Adsorption, becomes a viable alternative because of the reusable nature of the adsorbents used [2]. Particularly, pressure swing adsorption (PSA) processes for capturing CO_2 from fossil fuel combustion has been intensively studied [3–11]. Temperature swing adsorption (TSA) [12] and the combined processes of PSA and TSA [13] were also studied to capture carbon dioxide. Development of regenerable adsorbents that have high capacity, high selectivity and good regenerability of CO_2 adsorption/desorption is critical for the success of the adsorption process [14].

There exist many potential candidate adsorbent materials available to post-combustion CO_2 capture, which include carbonaceous materials [15], zeolite molecular sieves [16], metal organic framework materials [17], amine supported mesoporous materials [18], hydrotalcite-like compounds [19], limestone [20], lithium zirconate [21], lithium silicate [22], and other metal oxides materials [23]. Carbonaceous materials are promising adsorbents, since they have high surface area, good CO_2 adsorption capacity, they are water tolerant and they can be produced with novel morphologies (monolith, bead, fiber, granular, respectively). Additionally, they are less expensive than other adsorbents like zeolites [15]. Activated carbon (AC) bead is spherical; no binder material is used in producing AC bead. The spherical nature and hardness of AC bead minimizes dust formation and attrition losses during adsorption and regeneration processes. AC bead also exhibits excellent fluidization properties both in gas and liquid applications. These characteristics make AC bead the material of choice for higher performance in carbonaceous materials application.

The AC beads used here are pitch-based synthesized by State Key Laboratory in China [24]. The objective of this work is to measure fundamental properties of CO_2 adsorption in this new adsorbent such that an adsorption process can be designed for CO_2 capture from flue gases. Adsorption equilibrium of CO_2 and N_2 at 303, 333, 363, 393, and 423 K with pressures ranging from 0 to 100 kPa was gravimetrically measured on AC beads. Equilibrium of pure gases up to 4000 kPa was also measured at 303, 333 K. Furthermore, adsorption kinetics of pure CO_2 and N_2 on AC beads was stud-

* Corresponding author. Tel.: +351 22 508 1618; fax: +351 22 508 1674.
E-mail addresses: czshen@fe.up.pt, arodrig@fe.up.pt (A.E. Rodrigues).

1385-8947/$ – see front matter © 2010 Published by Elsevier B.V.
doi:10.1016/j.cej.2009.12.005

Nomenclature

a_i	number of neighboring sites occupied by adsorbate i molecule
A	first Virial coefficient (m^2/mol)
B	second Virial coefficient (m^4/mol^2)
C_i	gas phase concentration of component i (mol/m^3)
C_{i0}	feed concentration of component i entering the column (mol/m^3)
C_{ip}	gas concentration of component i in the macropores (mol/m^3)
D_{ax}	axial dispersion coefficient (m^2/s)
D_c	micropore diffusion coefficient (m^2/s)
D_c^0	limiting diffusion coefficient at infinite temperatures (m^2/s)
D_{ij}	binary molecular diffusivity (m^2/s)
D_k	Knudsen diffusivity (m^2/s)
D_m	molecular diffusion coefficient (m^2/s)
D_p	pore diffusivity (m^2/s)
E_a	activation energy of micropore diffusion (kJ/mol)
ERR	error function (%)
H	Henry constant (m^3/kg)
k_f	film mass transfer coefficient (m/s)
K_C	Henry constant (dimensionless)
K_H	Henry constant (mol/(kg kPa))
K_∞	adsorption constant at infinite temperature (mol/(kg kPa))
K_i	equilibrium constant of component i (Pa^{-1})
K_i^0	equilibrium constant of component i at infinite temperature (Pa^{-1})
L	column length (m)
m_{ads}	mass of adsorbed gas (kg)
m_s	mass of adsorbent (kg)
M_W	molecular weight of the gas (kg/mol)
P	pressure (Pa)
q	absolute adsorbed phase concentration (mol/kg)
q_{ex}	excess adsorbed phase concentration (mol/kg)
q_{cal}	calculated adsorbed phase concentration (mol/kg)
q_{exp}	experimental adsorbed phase concentration (mol/kg)
$q_{m,i}$	maximum amount adsorbed of component i (mol/kg)
q_s	adsorbed phase concentration in the crystal surface (mol/kg)
$\langle \overline{q_i} \rangle$	average amount adsorbed of component i (mol/kg)
$\overline{q_i}$	average amount adsorbed in the crystals (mol/kg)
r_c	crystal radius (m)
R_g	universal gas constant (J/(mol K))
R_p	pellet radius (m)
R_e	Reynolds number
S	adsorbent specific area (m^2/kg)
Sc	Schmidt number
Sh	Sherwood number
t	time (s)
$\bar{t}$	stoichiometric time (s)
T	temperature (K)
v	interstitial velocity (m/s)
V_{ads}	volume of adsorbed phase (m^3)
V_c	volume of the cell where the adsorbent is located (m^3)
V_s	volume of the solid adsorbent (m^3)
z	partition of the column length L (m)

Greek letters

Δm	difference of weight between two measurements (kg)
$(-\Delta H^0)$	heat of adsorption at zero coverage (kJ/mol)
$(-\Delta H)$	isosteric heat of adsorption (kJ/mol)
ε_c	column porosity
ε_p	pellet porosity
μ	gas viscosity (Pa s)
ρ_g	density of the gas phase (kg/m^3)
ρ_l	density of the adsorbed phase (kg/m^3)
ρ_p	density of the adsorbent (kg/m^3)
τ_g	pore tortuosity

ied by diluted breakthrough experiments. The experiments were performed over the same temperature range from 303 to 423 K.

2. Experimental

2.1. Activated carbon beads

Pitch-based AC beads were prepared from coal tar pitch, which was blended with naphthalene under stirring, and then heated in the atmosphere of nitrogen. The blended pitch was then pulverized into particles and pitch spheres were obtained using an emulsion method. Furthermore, stabilization, carbonization and activation of the spheres were followed. A detailed preparation procedure was given in a previous publication [24].

Scanning electron microscopy (SEM) was performed with a JEOL JSM-6360 LV (Japan) to a portion of the AC beads. The SEM image was recorded with 15 kV accelerating voltage and 50 times of magnification. The Mercury porosimetry was performed using a PoreMaster 60 Porosimeter (Quantachrome). The mercury intrusion–retraction was measured over a wide range of pressures 0.7–400,000 kPa. For a detailed determination of the micropore structure, the N_2 physisorption isotherm was measured at 77 K using an Autosorb-1 physisorption–chemisorption analyzer. The specific surface area has been calculated using Brunauer–Emmett–Teller (BET) method.

2.2. Adsorption equilibrium

Adsorption equilibrium measurements of pure gases were performed in a magnetic suspension microbalance (Rubotherm, Germany) operated in a closed system. The accuracy of the microbalance is about $\pm 2 \times 10^{-8}$ kg. Two Lucas Schaevitz pressure transducers were used, one from 0 to 100 kPa with an accuracy $\pm 2 \times 10^{-2}$ kPa and another from 0 to 25,000 kPa with an accuracy ±2.5 kPa to acquire data at low and high pressures, respectively. The degassing of the adsorbent was carried out under vacuum at 423 K overnight. Regeneration of the adsorbent for different experiments was only performed under vacuum at desired temperature. Isotherms of N_2 and CO_2 were measured at 303, 333, 363, 393, and 423 K in the range of 0–100 kPa and isotherms at 303, 333 K were also measured up to 4000 kPa. The reversibility of the isotherms was confirmed with adsorption and desorption measurements. Adsorption and desorption points are plotted in the same image since we have observed that the isotherms are reversible. The absolute amount adsorbed was calculated at the range 0–4000 kPa.

2.3. Kinetics

Kinetics of adsorption of pure gases was measured by diluted breakthrough curves of the pure gases (0.5% of CO_2 or N_2 diluted in

Table 1
Experimental conditions used for the measurement of CO_2 and N_2 diluted breakthrough curves.

Breakthrough curve experiments	
Column length (cm)	16.5
Column diameter (cm)	0.93
Flowrate (cm^3/min)	30.0[a]
Column porosity (–)	0.32
Mass of adsorbent (g)	7.44771
Feed composition (vol.%)	0.5% of adsorbate in He
Total pressure (kPa)	100
Temperature (K)	303, 333, 363, 393, and 423

[a] Measured at 293 K and atmospheric pressure

helium). An initial degassing of the sample was performed at 423 K under the flow of helium overnight, while regeneration was only carried out under a flow of helium. The column was placed in a GC oven (Varian CP 3800 Gas Chromatograph) to control the temperature of each experiment within ±0.1 K. A four-way valve was employed to switch between feed (adsorbate + helium) and inert gas (helium) for adsorption and desorption measurements, respectively. The breakthrough curves of CO_2 and N_2 were measured in the same temperature range employed in the equilibrium measurements. The outlet concentration was analyzed by a thermal conductivity detector (TCD). Experimental conditions employed in these measurements are detailed in Table 1.

All gases used in the experiments were supplied by Air Liquide (Portugal) with purities of: CO_2 > 99.998%, N_2 > 99.995% and He > 99.999%.

3. Theoretical

3.1. Adsorption equilibrium

The gravimetric method is a very accurate technique to measure adsorption equilibrium of pure gases. However, when the adsorbent is immersed within a fluid with a certain density, some buoyancy exists and should be taken into account to obtain the real or absolute amount adsorbed. The excess amount adsorbed q_{ex} is directly obtained from experimental measurements ($q_{ex} = \Delta m/m_s M_w$), while the absolute amount adsorbed cannot be obtained directly because it is not possible to measure the density of the adsorbed phase which is assumed to be equal to the density of the liquid at its boiling point at 1 atm [25]. Employing this correction, the final equation to calculate the absolute amount adsorbed from experimental data is [26]:

$$q = \frac{\Delta m + \rho_g (V_s + V_c)}{m_s M_w} \frac{\rho_l}{\rho_l - \rho_g} \tag{1}$$

where q is the absolute amount adsorbed, Δm is the difference of weight between one measurement and the previous one, ρ_g is the density of the gas, ρ_l is the density of the adsorbed phase, V_s is the volume of the solid adsorbent and V_c is the volume of the cell where the adsorbent is located, m_s is the mass of adsorbent used in the measurement, and M_w is the molecular weight of the gas. A calibration with helium was performed to determine the volumes that contribute to the buoyancy effect ($V_s + V_c$), under the assumption that this gas is not adsorbed ($m_{ads} = V_{ads} = 0$).

The Virial isotherm model was chosen to describe the adsorption equilibrium of pure gases on the activated carbon beads [27,28]. This model is thermodynamically correct at low and high coverages and is also very flexible to fit isotherms with different degrees of steepness in a wide range of pressure and temperature conditions [29]. The model is obtained by applying the bi-dimensional Virial equation of state to the Gibbs isotherm that results in [27,28]:

$$P = \frac{q}{K_H} \exp\left(\frac{2}{S} A q + \frac{3}{2S^2} B q^2 + \cdots\right) \tag{2}$$

where P is the pressure, S is the adsorbent specific surface area, A and B are Virial coefficients, and K_H is the Henry constant (mol g^{-1} kPa^{-1}), which has an exponential dependence with temperature described by Van't Hoff equation:

$$K_H = K_\infty \exp\left(-\frac{\Delta H^0}{R_g T}\right) \tag{3}$$

where K_∞ is the adsorption constant at infinite temperature, T is the temperature, (ΔH^0) is the heat of adsorption at zero coverage and R_g is the universal gas constant.

For many systems, such as adsorption of carbon dioxide and propane on H-mordenite, or adsorption of methane, ethane and carbon dioxide on activated carbon, the Virial equation can be truncated after the second Virial coefficient. The temperature dependence of the Virial coefficients was described by [27,28]:

$$A = \sum_{m=0}^{\infty} \frac{A_m}{T^m}, \quad B = \sum_{m=0}^{\infty} \frac{B_m}{T^m} \tag{4}$$

moreover, the Virial isotherm was extended for the prediction of multicomponent adsorption by Taqvi and LeVan [29].

An alternative model to fit the pure component and multicomponent data was the multisite Langmuir model. The multisite Langmuir model has been employed to fit adsorption data of a wide variety of gases in different adsorbents [26,30–33]. This theoretical model assumes that each adsorbate molecule can occupy more than one site on a homogeneous surface, with the same energies. Neglecting adsorbate-adsorbate interactions, the model can be expressed as [31]:

$$\frac{q_i}{q_{m,i}} = a_i K_i P \left(1 - \frac{q_i}{q_{m,i}}\right)^{a_i} \tag{5}$$

where $q_{m,i}$ is the maximum amount adsorbed of component i; a_i is the number of neighboring sites occupied by a molecule of component i, and K_i is the adsorption constant which has an exponential temperature dependence:

$$K_i = K_i^0 \exp\left(-\frac{\Delta H^0}{R_g T}\right) \tag{6}$$

where K_i^0 is the adsorption constant of component i at infinite T. In this model, the isosteric heat of adsorption is not a function of adsorbate loading. The saturation capacity of each component is imposed by the thermodynamic constraint $a_i q_{m,i}$ = constant.

Fitting of the Virial equations and multisite Langmuir to the absolute amount adsorbed was performed with MATLAB 7.4.0 (The Mathworks, Inc). The error function is defined by:

$$\text{ERR } (\%) = 100 \sum_T \sum_P \sum_i \left(\frac{q_{cal} - q_{\exp}}{q_{cal}}\right)^2 \tag{7}$$

where T is each experimental temperature, P is the pressure, i is the number of points of each isotherm, q_{cal} is the calculated amount adsorbed, and $q_{\exp}$ is the experimental amount adsorbed. The minimization routine used finds the minimum of the error function using the Nelder–Mead Simplex Method of direct search.

We have employed models with certain complexity to be fitted reason why we have employed the absolute amount adsorbed. However, other authors have fitted the excess amount adsorbed using the Langmuir model where the maximum value correspond to the saturation of pore walls [34]. In the present work, Langmuir model could not fit the data with enough accuracy.

3.2. Kinetics

In this work, we have measured breakthrough curves of pure gases (CO_2, N_2) with a very low partial pressure diluted in helium. Under such conditions, adsorbate isotherm is linear avoiding undesired effects of equilibrium nonlinearity in diffusivity determinations. Also, the heat generated by adsorption is small allowing us to assume isothermal operation. Furthermore, it can be assumed that no velocity variations occur during adsorption.

After obtaining the experimental data (breakthrough curves), the first thing to do is to calculate the stoichiometric time to compare with the capacity obtained by the dynamic method with the equilibrium one. The stoichiometric time can be calculated by [34]:

$$\bar{t} = \frac{L}{v}\left[1 + \left(\frac{1-\varepsilon_c}{\varepsilon_c}\right)K_C\right] = \int_0^\infty \left(1 - \frac{C}{C_0}\right)dt \tag{8}$$

where K_C is the dimensionless Henry constant; v is the interstitial gas velocity; L is the length of column; ε_c is the column porosity. By Eq. (8) we can obtain the Henry constant for a homogeneous particle that is related with the Henry constant by $K_C = \varepsilon_p + \rho_p H$.

For the analysis of the breakthrough curves we have considered the case of a column filled with a bidisperse adsorbent where the flow can be considered as an axially dispersed plug flow. Moreover, it was assumed that the process is isothermal and that the velocity is constant within the column.

The mass balance in a differential element of the column is given by [35,36]

$$\frac{\partial C_i}{\partial t} + \left(\frac{1-\varepsilon_c}{\varepsilon_c}\right)\rho_p \frac{\partial \left\langle \overline{q_i} \right\rangle}{\partial t} + \left(\frac{1-\varepsilon_c}{\varepsilon_c}\right)\varepsilon_p \frac{\left\langle C_{ip} \right\rangle}{\partial t} = -v\frac{\partial C_i}{\partial z} + D_{ax}\left(\frac{\partial^2 C_i}{\partial z^2}\right) \tag{9}$$

with initial condition:

$$C_i = 0 \tag{10}$$

and Danckwerts boundary conditions:

$$D_{ax}\left.\frac{\partial C_i}{\partial z}\right|_{(t,0)} = v(C_i - C_{i0}) \tag{11}$$

$$\left.\frac{\partial C_i}{\partial z}\right|_{(t,L)} = 0 \tag{12}$$

where C_i is the gas phase concentration of component i, ρ_p is the density of the pellet, $\left\langle C_{ip} \right\rangle$ is the pellet averaged concentration of component i in the macropores of the pellet, $\left\langle \overline{q_i} \right\rangle = (2/R_p^{(S+1)}\int_0^{R_p} q_i R^S dR)$ is the average amount adsorbed of component i, C_{i0} is the feed concentration of component i entering the column and D_{ax} is the axial dispersion.

The mass balance in a volume element of the pellet is represented by:

$$\varepsilon_p \frac{\partial C_{ip}}{\partial t} + \rho_p \frac{\partial \overline{q_i}}{\partial t} = \frac{1}{R^S}\frac{\partial}{\partial r}\left[\varepsilon_p D_p R^S \frac{\partial C_{ip}}{\partial R}\right] \tag{13}$$

with initial condition:

$$C_{ip(0,R)} = 0 \tag{14}$$

and boundary conditions:

$$\varepsilon_p D_p \left.\frac{\partial C_{ip}}{\partial R}\right|_{(t,R_p)} = k_f (C_i - \left. C_{ip}\right|_{(t,R_p)}) \tag{15}$$

$$\left.\frac{\partial C_{ip}}{\partial R}\right|_{(t,0)} = 0 \tag{16}$$

where ε_p is the pellet porosity, D_p is the pore diffusion coefficient, R_p is the pellet radius, k_f is the film mass transfer coefficient, C_{ip} is the gas concentration of component i in the macropores and $\overline{q_i} = (2/r_c^{(S+1)}\int_0^{r_c} q_i r^S dr)$ is the average amount adsorbed in the crystals. The sub-index S denotes the geometry of the pellet and has value of 0, 1 and 2 for infinite slab, infinite cylinder and spheres, respectively.

The mass balance in the micropores is described by:

$$\frac{\partial q_i}{\partial t} = \frac{1}{r^S}\frac{\partial}{\partial r}\left[D_c r^S \frac{\partial q_i}{\partial r}\right] \tag{17}$$

with initial condition:

$$q_{(0,r)} = 0 \tag{18}$$

and boundary conditions:

$$q_{(t,r_c)} = q_s = HC_{ip} \tag{19}$$

$$\left.\frac{\partial q}{\partial r}\right|_{(t,0)} = 0 \tag{20}$$

where D_c is the crystal or micropore diffusivity, r_c is the crystal radius and H is the Henry constant. In this work, linear isotherm was used to describe adsorption equilibrium because the partial pressure of adsorbate was very low.

In order to use the bidisperse model described by Eqs. (9)–(20), we need to calculate several mass transfer parameters like the axial dispersion coefficient, the film mass transfer resistance and pore diffusivity. The axial diffusion coefficient can be calculated by [34]:

$$D_{ax} = (0.45 + 0.55\varepsilon_c)D_m + 0.35R_p v \tag{21}$$

where D_m is the molecular diffusivity.

To calculate the film mass transfer coefficient, the correlation proposed by Wakao and Funazkri has been used [34]:

$$Sh = 2.0 + 1.1Re^{0.6}Sc^{1/3} \tag{22}$$

where $Sh = 2R_p k_f/D_m$ is the Sherwood number, $Re = 2\rho_g v R_p/\mu$ is the Reynolds number, and $Sc = \mu/\rho_g D_m$ is the Schmidt number.

The pore diffusivity was calculated with the Bosanquet equation:

$$\frac{1}{D_{p,i}} = \tau_p\left(\frac{1}{D_{m,i}} + \frac{1}{D_{k,i}}\right) \tag{23}$$

where $D_{k,i}$ is the Knudsen diffusivity and τ_p is the pore tortuosity. The molecular diffusivity for the mixture was approximated with:

$$D_{m,i} = \frac{1 - y_i}{\sum_{\substack{j=1 \\ j\neq i}}^{n} \frac{y_j}{D_{ij}}} \tag{24}$$

where the binary molecular diffusivities D_{ij} were calculated with the Chapman–Enskog equation [33]. The Knudsen diffusivity ($D_{k,i}$, m^2/s) was calculated by:

$$D_{k,i} = 9700 r_p \sqrt{\frac{T}{M_W}} \tag{25}$$

where r_p is the mean macropore radius (cm).

The micropore diffusivity D_c is an activated process with exponential dependence with temperature according to:

$$\frac{D_c}{r_c^2} = \frac{D_c^0}{r_c^2}\exp\left(-\frac{E_a}{R_g T}\right) \tag{26}$$

where D_c^0/r_c^2 is the limiting diffusivity (divided by r_c^2) at infinite temperature and E_a is the activation energy.

Simulations of the mathematical model presented above were performed in gPROMS (PSE Enterprise, UK) using the orthogonal collocation on finite elements (OCFEM). The number of elements used was 25 with two interior collocation points (third order polynomials) in each element of the adsorption bed, and 10 finite elements for the pellet and for the crystal, with two internal collocation points in each domain.

4. Results and discussion

4.1. Activated carbon beads

A SEM image of the AC beads is shown in Fig. 1. Particle sizes with narrow range can be observed. The mercury porosimetry was employed to determine the macroporous structure of the AC beads. Macropore size distribution of the AC bead resulted from mercury porosimetry can be observed in Fig. 2. The porosimetry showed some quite large pores (>100 μm) and macropores with average diameter of 0.4042 μm. Also, some mesopores (<0.01 μm) were observed. Nitrogen adsorption isotherm at 77 K and the micropore size distribution (calculated using Barrer-Joyner-Halenda method) are shown in Fig. 3. The results show a large amount of micropores, resulting in a high BET specific surface area of 845.87 m^2/g.The summary of characteristic parameters was shown in Table 2.

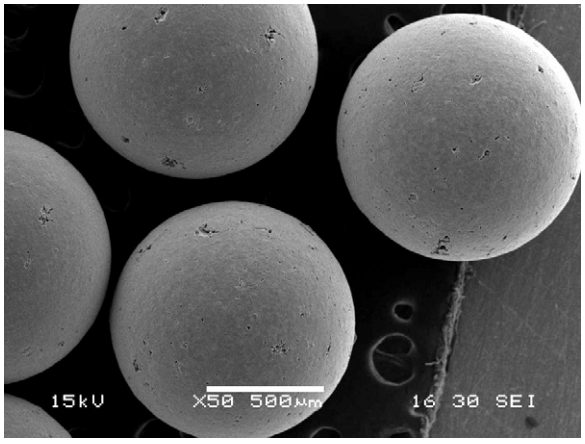

Fig. 1. Scanning electron microscopy of activated carbon beads made of coal tar pitch.

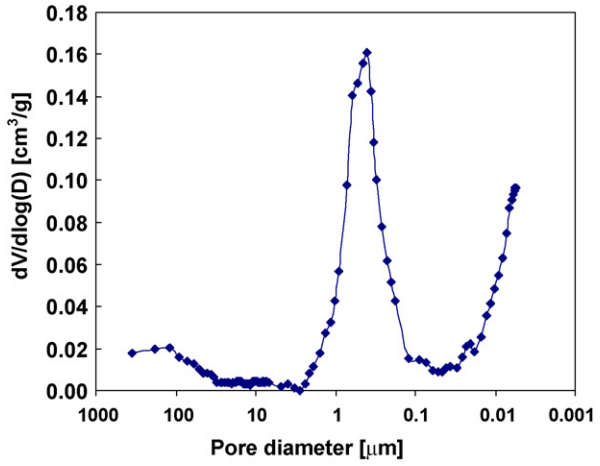

Fig. 2. Macropore size distribution of the pitch-based activated carbon beads determined by mercury intrusion.

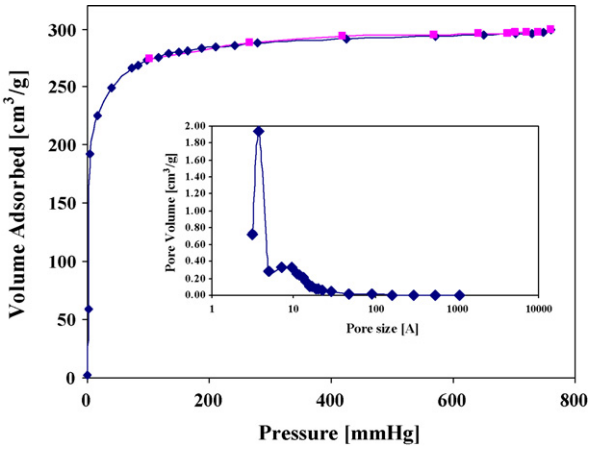

Fig. 3. N_2 adsorption isotherm at 77 K and micropore size distribution of the activated carbon beads.

Table 2
Characteristic parameters of pitch-based activated carbon (AC) beads.

Specific surface area (m^2/g)	845.87
Pellet density (g/ml)	0.9843[a]
Solid density (g/ml)	1.9908[b]
Pellet void fraction	0.506
bead diameter (mm)	1–1.18

[a] Measured at 3.58 kPa.
[b] Determined by helium pycnometry.

4.2. Adsorption equilibrium

We have calculated the absolute amount adsorbed using the buoyancy correction described in Eq. (1). An example of the difference between absolute amount adsorbed and excess amount adsorbed is shown in Fig. 4. Small difference can be observed at low pressure, which allows making the assumption that the buoyancy corrections are negligible in this range (the density of the gas phase is very small if compared with the density of the adsorbed phase). At higher pressures, the difference becomes significant. The main reason for this difference is that the volume of the adsorbed layer is not negligible and also the gas density becomes closer to the density of the adsorbed layer at higher pressure.

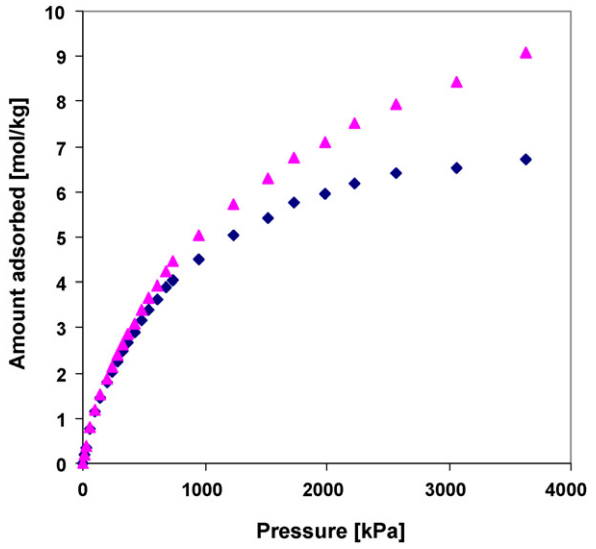

Fig. 4. Carbon dioxide adsorption equilibrium on pitch-based AC beads at 333K. ▲, absolute amount adsorbed, q; ♦, excess amount adsorbed, q_{ex}.

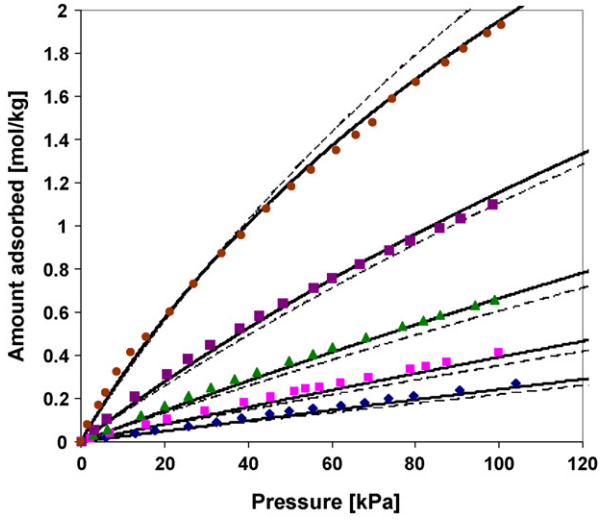

Fig. 5. Carbon dioxide adsorption equilibrium on pitch-based AC beads at the pressure range of 0–100 kPa. ●, T = 303 K; ■, T = 333 K; ▲, T = 363 K; ■, T = 393 K; ♦, T = 423 K; solid lines, Virial model; dotted lines, multisite Langmuir model.

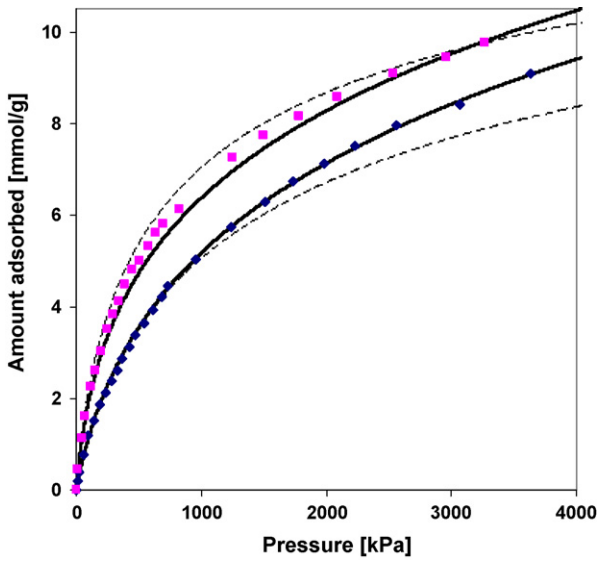

Fig. 7. Carbon dioxide adsorption equilibrium on pitch-based AC beads. ■, T = 303 K; ♦, T = 333 K; solid lines, Virial model; dotted lines, multisite Langmuir model.

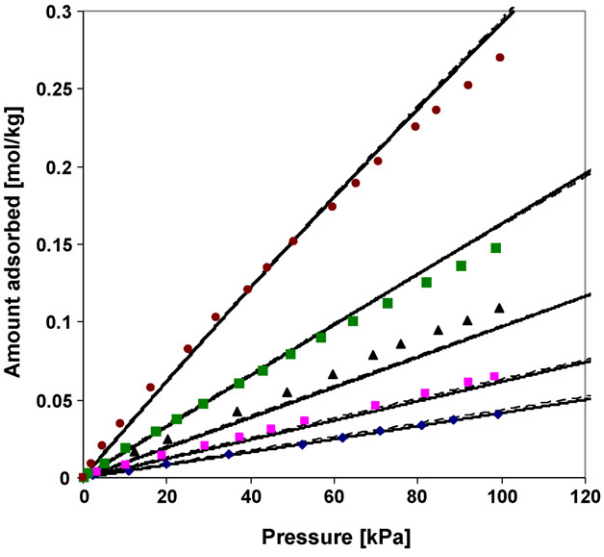

Fig. 6. Nitrogen adsorption equilibrium on pitch-based AC beads. ●, T = 303 K; ■, T = 333 K; ▲, T = 363 K; ■, T = 393 K; ♦, T = 423 K; solid lines, Virial model; dotted lines, multisite Langmuir model.

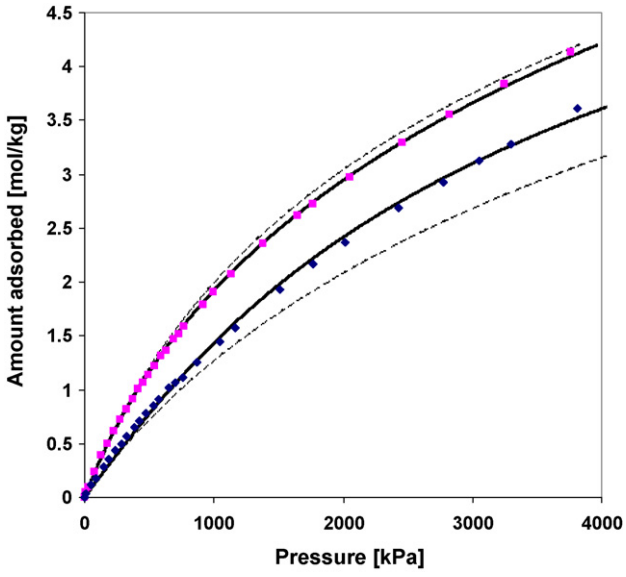

Fig. 8. Nitrogen adsorption equilibrium on pitch-based AC beads. ■, T = 303 K; ♦, T = 333 K; solid lines, Virial model; dotted lines, multisite Langmuir model.

Since activated carbon is usually used as adsorbent at low-pressure range, a wide temperature range ranging 0–100 kPa were measured in this work and from these equilibrium points at very low pressure where isotherms were linear, Henry constant can be accurately estimated. Equilibria ranging from 0 to 4000 kPa was measured to determine the equilibrium behavior of this AC beads at high pressure.

The adsorption equilibrium isotherms (absolute amount adsorbed per mass of adsorbent) of CO_2, N_2 at 303, 333, 363, 393, and 423 K at low pressures and at 303, 333 K at higher pressures were presented in Figs. 5–8, respectively. All isotherms were completely reversible. Preferential adsorption of CO_2 on this AC beads can be seen from the equilibrium isotherms. The selectivity toward carbon dioxide decreases when increasing the pressure (see Fig. 9). The CO_2/N_2 loading ratio was calculated by q_{CO_2}/q_{N_2} for the same partial pressures.

In Figs. 5–8 the solid lines represent the Virial fitting of the data. It can be observed that the quality of the fitting is very good at low and high pressures. The parameters of the fittings are reported in Table 3 and can be employed in the prediction of multicomponent adsorption equilibrium to design a PSA unit using the multicomponent extension of the Virial model [27,28].

Table 3
Fitting parameters of the Virial model of CO_2 and N_2 for pitch-based activated carbon.

Gas	K_∞ [mol/(kg kPa)]	$(-\Delta H^0)$ (kJ/mol)	A_0 (kg/mol)	A_1 [(kg K)/mol]	B_0 [(kg/mol)^2]	B_1 [(kg/mol)^2 K]
CO_2	3.41×10^{-6}	23.17	6.889	−0.0871	0.0244	−8.652
N_2	2.38×10^{-6}	18.11	−2.017	688.392	0.348	−105.164

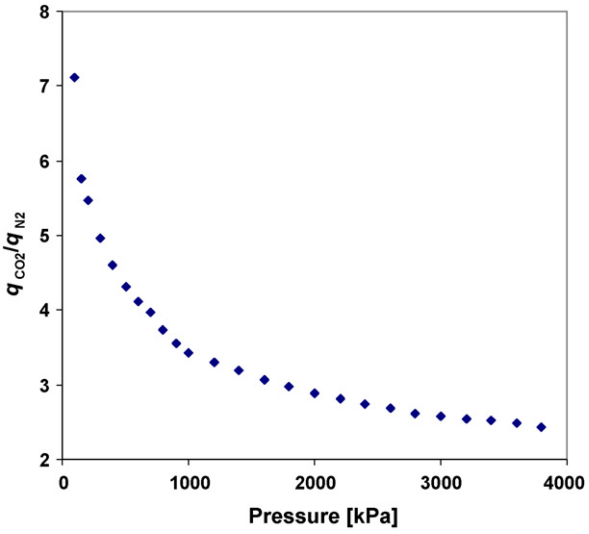

Fig. 9. CO_2/N_2 loading ratio at constant partial pressure calculated from single components as a function of pressure at 303 K.

Table 4
Fitting parameters of the multisite Langmuir model for CO_2 and N_2 on pitch-based activated carbon.

Gas	K_0^i (kPa^{-1})	$(-\Delta H^0)$ (kJ/mol)	$q_{m,i}$ (mol/kg)	a_i
CO_2	6.06×10^{-8}	23.16	17.66	2.90
N_2	5.88×10^{-8}	17.50	15.47	3.31

A second analysis was performed using multisite Langmuir model (dotted lines in Figs. 5–8). The parameters of the fitting are reported in Table 4. The thermodynamic restriction of the $a_i q_{\max,i}$ = constant was satisfied in the fitting. In Figs. 5–8, we can observe that the fitting of multisite Langmuir model is good at low pressures 0–100 kPa, but has poor consistency with experimental data at high pressures. One possible reason is that the isosteric heat of adsorption is assumed to be independent of adsorbate loading, while actually the isosteric heat of adsorption varies with the coverage, as shown in Fig. 10. We have presented two different analyses to attend different possibilities of process design; the Virial model may be suitable when water is present in the system

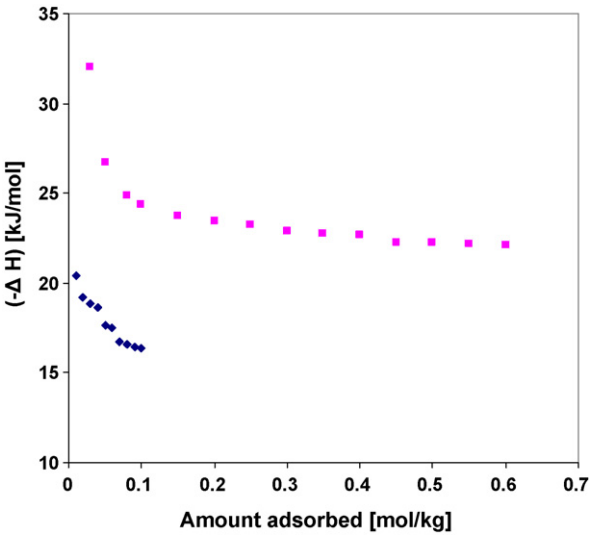

Fig. 10. Isosteric heat of adsorption of carbon dioxide and nitrogen on pitch-based AC beads. ■, carbon dioxide; ♦, nitrogen.

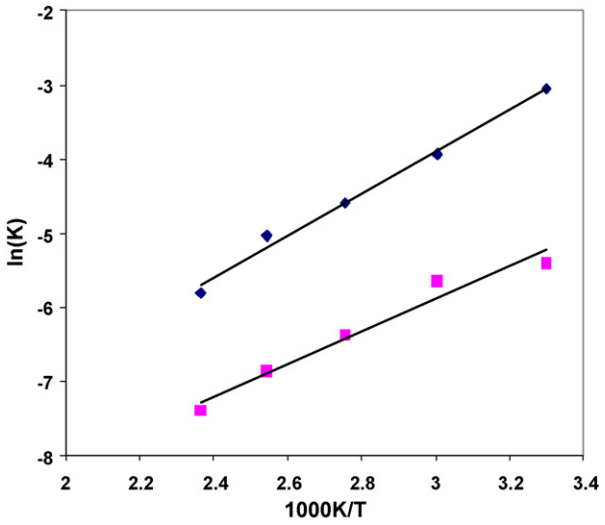

Fig. 11. Van't Hoff plot of Henry constants against the reciprocal of temperature. ♦, carbon dioxide, $(-\Delta H_{CO_2}) = 23.403$ kJ/mol; ■, nitrogen, $(-\Delta H_{N_2}) = 18.150$ kJ/mol.

and the isotherm shape cannot be well described with the multisite Langmuir model.

Isosteric heats of adsorption as a function of surface coverage were calculated using isotherms at different temperatures ranging from 0 to 100 kPa. The Clausius–Clapeyron equation described as below was utilized in these calculations:

$$\frac{(-\Delta H)}{RT^2} = \left[\frac{\partial \ln P}{\partial T}\right]_q \quad (27)$$

where $(-\Delta H)$ is the isosteric heat of adsorption at specific loading. The result was shown in Fig. 10. It can be observed that the isosteric heat of adsorption varies with the surface loading, indicating that the AC beads has energetically heterogeneous surface. Knowledge of the magnitude of the isosteric heat of adsorption and its variation with coverage can provide useful information concerning the nature of the surface and the adsorbed phase.

The limiting heat of adsorption at zero coverage, as calculated from the slopes of the Van't Hoff plots of the Henry's law constants against the reciprocal of temperatures [35,36], is shown in Fig. 11. The absolute amount adsorbed of CO_2 and N_2 on this AC beads and the limiting heat of adsorption at zero coverage were compared with those on other activated carbons reported previously in literature and summarized in Table 5. The equilibrium data obtained is in agreement with some data available in literature, while the value of limiting heat of adsorption at zero coverage also compares very well with other activated carbons [37], such as Norit R1 Extra (22.0 kJ/mol), BPL (25.7 kJ/mol) and Maxsorb (16.2 kJ/mol) presented in previous literature.

4.3. Kinetics

All adsorption units are dynamic separation process and thus it is very important to measure the velocity of diffusion of the gases in the porous structure of the adsorbent. In this work, the diffusion of single gases in AC beads was studied by diluted breakthrough experiments. Breakthrough curves of CO_2, N_2 at 303, 333, 363, 393, and 423 K are shown in Figs. 12 and 13, respectively. The solid lines represent the fitting with the bidisperse model, using D_c/r_c^2 as the only fitting parameter.

The stoichiometric time was calculated using Eq. (8). The comparison between the Henry constant obtained from the dynamic and gravimetric methods is shown in Table 6 for both CO_2 and N_2.

Table 5
Comparison of adsorption equilibrium of CO_2 and N_2 on different activated carbons.

Activated carbons	Adsorbate	q (mol/kg)	P (MPa)	T (K)	$(-\Delta H^0)$ (kJ/mol)	Literature
Commercial sample	CO_2	7.492	2.132	303	–	[38]
	N_2	1.086	4.886	303	–	[38]
G32-H	CO_2	5.318	2.074	298	28.00	[14]
	N_2	2.106	1.939	298	–	[14]
JX101	N_2	1.735	0.981	298	–	[39]
Norit R 1 Extra	CO_2	10.32	3.030	298	22.0	[37]
	CO_2	11.270	6.000	298	–	[25]
	N_2	4.438	5.980	298	–	[25]
BPL	CO_2	7.345	4.821	298	25.7	[37]
	CO_2	7.28	3.450	301	–	[40]
Maxsorb	CO_2	25.802	4.586	298	16.2	[40]
	CO_2	2.164	0.094	301	–	[41]
Norit RB2	CO_2	9.527	3.024	298	–	[42]

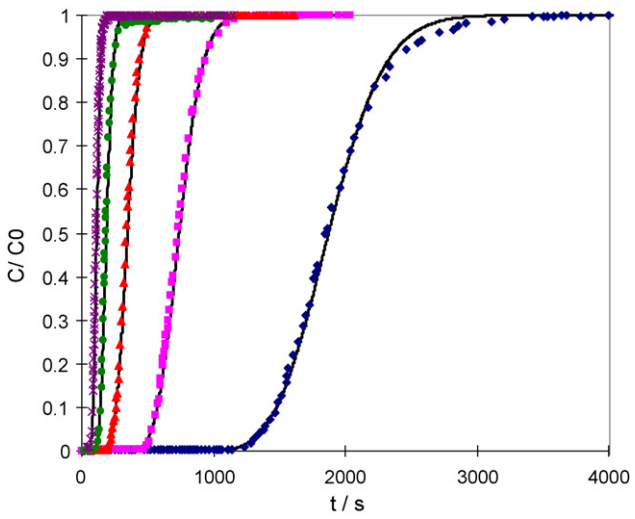

Fig. 12. Diluted breakthrough curves of CO_2 in AC beads at 303, 333, 363, 393 and 423 K. *, T = 423 K; ●, T = 393 K; ▲, T = 363 K; ■, T = 333 K; ♦, T = 303 K; solid lines represent the bidisperse model of Eqs. (20)–(31).

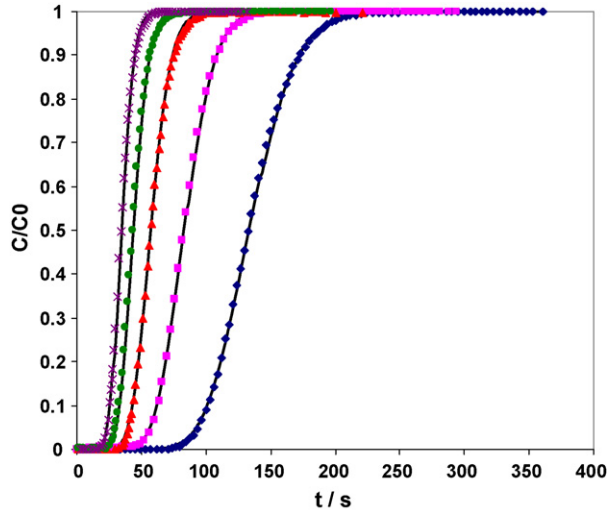

Fig. 13. Diluted breakthrough curves of N_2 in pitch-based AC beads at 303, 333, 363, 393 and 423 K. *, T = 423 K; ●, T = 393 K; ▲, T = 363 K; ■, T = 333 K; ♦, T = 303 K; solid lines represent the bidisperse model of Eqs. (20)–(31).

Table 6
Comparison of Henry constants of CO_2 and N_2 on pitch-based activated carbon beads calculated from isotherms and breakthrough curves.

T (K)	$K_{isotherms} \times 10^2$ [mol/(kg kPa)]	$K_{dynamic} \times 10^2$ [mol/(kg kPa)]	Error (%)
CO_2			
303	4.7163	5.1155	7.80
333	1.9342	2.0126	3.89
363	1.0199	0.9405	7.78
393	0.5501	0.5368	2.42
423	0.3026	0.3004	0.72
N_2			
303	0.3847	0.3564	7.35
333	0.1986	0.2178	8.81
363	0.1355	0.1463	7.38
393	0.1041	0.1092	4.67
423	0.0796	0.0848	6.13

Note that the error is less than 10%. It is very important to accurately measure the Henry constant since it provides essential information for prediction of multicomponent adsorption equilibrium [43].

In order to fill the parameters of the bidisperse model, diffusion parameters have to be given which can be determined once capacity is checked. The axial dispersion, film mass transfer coefficient and the micropore diffusivity are calculated from Eqs. (21) to (26). To estimate the pore diffusivity coefficient by the Bosanquet equa-

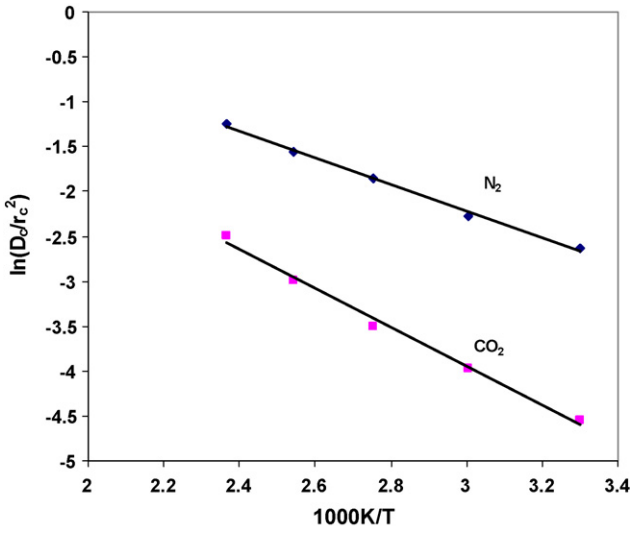

Fig. 14. Temperature dependence of micropore diffusivity of ■, CO_2; and ♦, N_2 in the AC beads between 303 and 423 K.

Table 7
Mass transfer parameters used for modeling diluted CO_2 and N_2 breakthrough curves in pitch-based AC beads. The value of D_c/r_c^2 was obtained from fitting while others were calculated.

T (K)	303	333	363	393	423
CO_2					
D_{ax} (cm^2/s)	0.356	0.414	0.475	0.555	0.606
D_m (cm^2/s)	0.505	0.592	0.684	0.782	0.884
D_k (cm^2/s)	0.048	0.050	0.0528	0.0549	0.057
D_p (cm^2/s)	2.201×10^{-2}	2.329×10^{-2}	2.45×10^{-2}	2.57×10^{-2}	2.677×10^{-2}
k_f (cm/s)	9.402	11.015	12.721	14.538	16.428
D_c/r_c^2 (s^{-1})	1.058×10^{-2}	1.885×10^{-2}	3.007×10^{-2}	5.060×10^{-2}	8.271×10^{-2}
N_2					
D_{ax} (cm^2/s)	0.418	0.486	0.557	0.632	0.711
D_m (cm^2/s)	0.606	0.710	0.8194	0.935	1.056
D_k (cm^2/s)	0.060	0.063	0.066	0.069	0.071
D_p (cm^2/s)	2.749×10^{-2}	2.91×10^{-2}	3.062×10^{-2}	3.207×10^{-2}	3.346×10^{-2}
K_f (cm/s)	11.379	13.307	15.350	17.503	19.764
D_c/r_c^2 (s^{-1})	7.185×10^{-2}	1.026×10^{-1}	1.573×10^{-1}	2.111×10^{-1}	2.867×10^{-1}

tion, a tortuosity factor of 2 was assumed for activated carbon [38]. The diffusion parameters used for the fitting of carbon dioxide and nitrogen are listed in Table 7.

According to the experimental results it was determined that micropore resistances control the diffusion mechanism for both CO_2 and N_2. At all temperatures, the diffusivities of nitrogen were much faster than carbon dioxide, as can be observed from Figs. 12 and 13. An exponential dependence of the micropore diffusivity with temperature is shown in Fig. 14 for CO_2 and N_2. The exponential dependence of the diffusion coefficient seems to correctly describe the experimental data within the temperature range studied. From the correlation, the value of D_c^0/r_c^2 and E_a can be determined for CO_2 and N_2.

5. Conclusions

Adsorption equilibrium for CO_2 and N_2 were gravimetrically measured at 303, 333, 363, 393, and 423 K ranging from 0 to 100 kPa and at 303, 333 K ranging from 0 to 4000 kPa on activated carbon (AC) beads. The data were well fitted with the Virial isotherm model both at low and high pressures, while the multisite Langmuir model only fits well with the data at low pressures. The adsorption capacity is 1.918 mol/kg for CO_2 and 0.270 mol/kg for N_2 at 303 K and 100 kPa. Carbon dioxide is preferentially adsorbed, which makes it a promising candidate for CO_2 separation from flue gas.

Diffusion of the gases in AC beads was studied by diluted breakthrough curves at the same range of temperature. The micropore diffusivity divided by $r_c^2 (D_c/r_c^2)$ for carbon dioxide and nitrogen obtained at 303 K is 1.058×10^{-2} and 7.185×10^{-2} s^{-1}, respectively. For both CO_2 and N_2 at all temperatures, micropore resistances control the diffusion within the AC beads. The diffusion of N_2 is much faster than CO_2.

The data provided in this work allows modeling of adsorption processes such as pressure swing adsorption (PSA) and temperature swing adsorption (TSA) for separation of CO_2 and N_2 in a wide pressure and temperature ranges using the pitch-based activated carbon beads.

Acknowledgments

The authors are grateful for the financial support of China 863 program (Grant No. 2008AA062302), Shanghai International Cooperation Project (Grant No. 08160704000), Shanghai Pujiang Talent program (Grant No. 08PJ14034) and the fellowship from China Scholarship Council (CSC) for the stay of C.S. at LSRE. The authors also acknowledge Professor Ling Licheng to provide the activated carbon beads.

References

[1] Working Group III of the Intergovernmental Panel on Climate Chage, IPCC Special Report on Carbon dioxide Capture and Storage, Cambridge University Press, 2005.
[2] J.P. Ciferno, T.E. Fout, A.P. Jones, J.T. Murphy, Capturing carbon from existing coal-fired power plants, Chem. Eng. Prog. 105 (4) (2009) 33–41.
[3] C.T. Chou, C.Y. Chen, Carbon dioxide recovery by vacuum swing adsorption, Sep. Purif. Technol. 39 (1–2) (2004) 51–65.
[4] K.T. Chue, J.N. Kim, Y.J. Yoo, S.H. Cho, R.T. Yang, Comparison of activated carbon and zeolite 13X for CO_2 recovery from flue-gas by pressure swing adsorption, Ind. Eng. Chem. Res. 34 (2) (1995) 591–598.
[5] B.K. Na, K.K. Koo, H.M. Eum, H. Lee, H.K. Song, CO_2 recovery from flue gas by PSA process using activated carbon, Korean J. Chem. Eng. 18 (2) (2001) 220–227.
[6] P. Xiao, J. Zhang, P. Webley, G. Li, R. Singh, R. Todd, Capture of CO_2 from flue gas streams with zeolite 13X by vacuum-pressure swing adsorption, Adsorption 14 (4–5) (2008) 575–582.
[7] M.T. Ho, G.W. Allinson, D.E. Wiley, Reducing the cost of CO_2 capture from flue gases using pressure swing adsorption, Ind. Eng. Chem. Res. 47 (14) (2008) 4883–4890.
[8] E.S. Kikkinides, R.T. Yang, S.H. Cho, Concentration and recovery of CO_2 from flue-gas by pressure swing adsorption, Ind. Eng. Chem. Res. 32 (11) (1993) 2714–2720.
[9] D. Ko, R. Siriwardane, L.T. Biegler, Optimization of a pressure-swing adsorption process using zeolite 13X for CO_2 sequestration, Ind. Eng. Chem. Res. 42 (2) (2003) 339–348.
[10] S.P. Reynolds, A.D. Ebner, J.A. Ritter, New pressure swing adsorption cycles for carbon dioxide sequestration, Adsorption 11 (2005) 531–536.
[11] A.L. Chaffee, G.P. Knowles, Z. Liang, J. Zhany, P. Xiao, P.A. Webley, CO_2 capture by adsorption: materials and process development, Int. J. Greenhouse Gas Contr. 1 (1) (2007) 11–18.
[12] J. Merel, M. Clausse, F. Meunier, Carbon dioxide capture by indirect thermal swing adsorption using 13X zeolite, Environ. Prog. 25 (4) (2006) 327–333.
[13] M. Ishibashi, H. Ota, N. Akutsu, S. Umeda, M. Tajika, J. Izumi, A. Yasutake, T. Kabata, Y. Kageyama, Technology for removing carbon dioxide from power plant flue gas by the physical adsorption method, Energy Convers. Manage. 37 (6–8) (1996) 929–933.
[14] R.V. Siriwardane, M.S. Shen, E.P. Fisher, J.A. Poston, Adsorption of CO_2 on molecular sieves and activated carbon, Energy Fuels 15 (2) (2001) 279–284.
[15] M. Radosz, X.D. Hu, K. Krutkramelis, Y.Q. Shen, Flue-gas carbon capture on carbonaceous sorbents: toward a low-cost multifunctional carbon filter for "green" energy producers, Ind. Eng. Chem. Res. 47 (10) (2008) 3783–3794.
[16] N. Konduru, P. Lindner, N.M. Assaf-Anad, Curbing the greenhouse effect by carbon dioxide adsorption with zeolite 13X, AlChE J. 53 (12) (2007) 3137–3143.
[17] A.R. Millward, O.M. Yaghi, Metal–organic frameworks with exceptionally high capacity for storage of carbon dioxide at room temperature, J. Am. Chem. Soc. 127 (51) (2005) 17998–17999.
[18] X.W. Liu, L. Zhou, X. Fu, Y. Sun, W. Su, Y.P. Zhou, Adsorption and regeneration study of the mesoporous adsorbent SBA-15 adapted to the capture/separation of CO_2 and CH_4, Chem. Eng. Sci. 62 (4) (2007) 1101–1110.
[19] M.K.R. Reddy, Z.P. Xu, G.Q. Lu, J.C.D. Da Costa, Layered double hydroxides for CO_2 capture: structure evolution and regeneration, Ind. Eng. Chem. Res. 45 (22) (2006) 7504–7509.
[20] H. Lu, E.P. Reddy, P.G. Smirniotis, Calcium oxide based sorbents for capture of carbon dioxide at high temperatures, Ind. Eng. Chem. Res. 45 (11) (2006) 3944–3949.
[21] E. Ochoa-Fernandez, M. Ronning, T. Grande, D. Chen, Nanocrystalline lithium zirconate with improved kinetics for high-temperature CO_2 capture, Chem. Mater. 18 (6) (2006) 1383–1385.

[22] T. Yamaguchi, T. Niitsuma, B.N. Nair, K. Nakagawa, Lithium silicate based membranes for high temperature CO_2 separation, J. Membr. Sci. 294 (1–2) (2007) 16–21.
[23] Q. Yang, Y.S. Lin, Kinetics of carbon dioxide sorption on perovskite-type metal oxides, Ind. Eng. Chem. Res. 45 (18) (2006) 6302–6310.
[24] Z.C. Liu, L.C. Ling, W.M. Qiao, L. Liu, Preparation of pitch-based spherical activated carbon with developed mesopore by the aid of ferrocene, Carbon 37 (4) (1999) 663–667.
[25] F. Dreisbach, R. Staudt, J.U. Keller, High pressure adsorption data of methane, nitrogen, carbon dioxide and their binary and ternary mixtures on activated carbon, Adsorption 5 (3) (1999) 215–227.
[26] S. Cavenati, C.A. Grande, A.E. Rodrigues, Adsorption equilibrium of methane, carbon dioxide, and nitrogen on zeolite 13X at high pressures, J. Chem. Eng. Data 49 (4) (2004) 1095–1101.
[27] R.M. Barrer, Sorption in porous crystals: equilibria and their interpretation, J. Chem. Technol. Biotechnol. 31 (2) (1981) 71–85.
[28] A.V. Kiselev, Vapor adsorption on zeolites considered as crystalline specific adsorbents, Adv. Chem. Ser. 102 (1971) 37–68.
[29] S.M. Taqvi, M.D. LeVan, Virial description of two-component adsorption on homogeneous and heterogeneous surfaces, Ind. Eng. Chem. Res. 36 (6) (1997) 2197–2206.
[30] C.A. Grande, V.M.T.M. Silva, C. Gigola, A.E. Rodrigues, Adsorption of propane and propylene onto carbon molecular sieve, Carbon 41 (13) (2003) 2533–2545.
[31] T. Nitta, T. Shigetomi, M. Kurooka, T. Katayama, An adsorption isotherm of multi-site occupancy model for homogeneous surface, J. Chem. Eng. Jpn. 17 (1) (1984) 39–45.
[32] J.A.C. Silva, A.E. Rodrigues, Multisite Langmuir model applied to the interpretation of sorption of n-paraffins in 5A zeolite, Ind. Eng. Chem. Res. 38 (6) (1999) 2434–2438.
[33] R.P. Ribeiro, T.P. Sauer, F.V. Lopes, R.F. Moreira, C.A. Grande, A.E. Rodrigues, Adsorption of CO_2, CH_4, and N_2 in activated carbon honeycomb monolith, J. Chem. Eng. Data 53 (10) (2008) 2311–2317.
[34] J. Bae, S.K. Bhatia, High-pressure adsorption of methane and carbon dioxide on coal, Energy Fuels 20 (2006) 2599–2607.
[35] D.M. Ruthven, Principles of Adsorption and Adsorption Processes, John Wiley & Sons, New York, 1984.
[36] R.T. Yang, Gas Separation by Adsorption Processes, Butterworths, Boston, 1987.
[37] S. Himeno, T. Komatsu, S. Fujita, High-pressure adsorption equilibria of methane and carbon dioxide on several activated carbons, J. Chem. Eng. Data 50 (2) (2005) 369–376.
[38] C.A. Grande, F.V.S. Lopes, A.M. Ribeiro, J.M. Loureiro, A.E. Rodrigues, Adsorption of off-gases from steam methane reforming (H_2, CO_2, CH_4, CO and N_2) on activated carbon, Sep. Sci. Technol. 43 (6) (2008) 1338–1364.
[39] Q. Wu, L. Zhou, J.Q. Wu, Y.P. Zhou, Adsorption equilibrium of the mixture $CH_4 + N_2 + H_2$ on activated carbon, J. Chem. Eng. Data 50 (2) (2005) 635–642.
[40] A.L. Hines, S.L. Kuo, N.H. Dural, A new analytical isotherm equation for adsorption on heterogeneous adsorbents, Sep. Sci. Technol. 25 (7–8) (1990) 869–888.
[41] V. Goetz, O. Pupier, A. Guillot, Carbon dioxide-methane mixture adsorption on activated carbon, Adsorption 12 (1) (2006) 55–63.
[42] Z. Yong, V.G. Mata, A.E. Rodrigues, Adsorption of carbon dioxide on chemically modified high surface area carbon-based adsorbents at high temperature, Adsorp.-J. Int. Adsorp. Soc. 7 (1) (2001) 41–50.
[43] O. Talu, Needs, status, techniques and problems with binary gas adsorption experiments, Adv. Colloid Interface Sci. 76 (1998) 227–269.